Spectrally Accurate Causality Enforcement Using SVD-based Fourier Continuations for High Speed Digital Interconnects

Lyudmyla L. Barannyk, *Member, IEEE,* Hazem A. Aboutaleb, Aicha Elshabini, *Fellow, IEEE & Fellow, IMAPS,* and Fred D. Barlow, *Senior Member, IEEE & Fellow, IMAPS*

***Abstract*—We introduce an accurate and robust technique for accessing causality of network transfer functions given in the form of bandlimited discrete frequency responses. These transfer functions are commonly used to represent the electrical response of high speed digital interconnects used on chip and in electronic package assemblies. In some cases small errors in the model development lead to non-causal behavior that does not accurately represent the electrical response and may lead to a lack of convergence in simulations that utilize these models. The approach is based on Hilbert transform relations or Kramers-Krönig dispersion relations and a construction of causal Fourier continuations using a regularized singular value decomposition (SVD) method. Given a transfer function, non-periodic in general, this procedure constructs highly accurate Fourier series approximations on the given frequency interval by allowing the function to be periodic in an extended domain. The causality dispersion relations are enforced spectrally and exactly. This eliminates the necessity of approximating the transfer function behavior at infinity and explicit computation of the Hilbert transform. We perform the error analysis of the method and take into account a possible presence of a noise or approximation errors in data. The developed error estimates can be used in verifying causality of the given data. The performance of the method is tested on several analytic and simulated examples that demonstrate an excellent accuracy and reliability of the proposed technique in agreement with the obtained error estimates. The method is capable of detecting very small localized causality violations with amplitudes close to the machine precision.**

***Index Terms*—Causality, dispersion relations, Kramers-Krönig relations, Fourier continuation, periodic continuation, Hilbert transform, least squares solution, regularized SVD, high speed interconnects.**

I. Introduction

The design of high speed interconnects that are common on chip and at the package level in digital systems, requires systematic simulations at different levels in order to evaluate the overall electrical system performance and avoid signal and power integrity problems [1]. To conduct such simulations, one needs suitable models that capture the relevant electromagnetic phenomena that affect the signal and power quality. These models are often obtained either from direct measurements or electromagnetic simulations in the form of discrete port frequency responses that represent scattering, impedance, or admittance transfer functions or transfer matrices in scalar or multidimensional cases, respectively. Once frequency responses are available, a corresponding macromodel can be derived using several techniques such as the Vector Fitting [2], the Orthonormal Vector Fitting [3], the Delay Extraction-Based Passive Macromodeling [4] among others. However, if the data are contaminated by errors, it may not be possible to derive a good model. These errors may be due to a noise, inadequate calibration techniques or imperfections of the test set-up in case of direct measurements or approximation errors due to the meshing techniques, discretization errors and errors due to finite precision arithmetic occurring in numerical simulations. Besides, these data are typically available over a finite frequency range as discrete sets with a limited number of samples. All this may affect the performance of the macromodeling algorithm resulting in non-convergence or inaccurate models. Often the underlying cause of such behavior is the lack of causality in a given set of frequency responses [5].

Causality can be characterized either in the time domain or the frequency domain. In the time domain, a system is said to be causal if the effect always follows the cause. This implies that a time domain impulse response function $h(t) = 0$ for $t < 0$, and a causality violation is stated if any nonzero value of $h(t)$ is found for some $t < 0$. To analyze causality, one can convert the frequency responses to the time domain using the inverse discrete Fourier transform. This approach suffers from the well known Gibbs phenomenon that is inherent for functions that are not smooth enough and represented by a truncated Fourier series. Examples of such functions include impulse response functions of typical interconnects that have jump discontinuities and whose spectrum is truncated since the frequency response data are available only on a finite length frequency interval. Direct application of the inverse discrete Fourier transform to raw frequency response data causes severe over and under shooting near the singularities. This problem is usually addressed by windowing the Fourier data to deal with the slow decay of the Fourier spectrum [6, Ch. 7]. Windowing can also be applied in the Laplace domain [7] to respect causality. This approach is shown to be more accurate and efficient than the Fourier approach [8]. There are other filtering techniques that deal with the Gibbs phenomenon but they require some knowledge of location of singularities (see [9], [10], [11], [12] and references therein). A related

Lyudmyla L. Barannyk is with the Department of Mathematics, University of Idaho, Moscow, ID 83844, USA (e-mail: barannyk@uidaho.edu).

Hazem A. Aboutaleb is with the Egyptian Communication and Cryptography Research Center, the Egyptian Armed Forces, Cairo, Egypt (e-mail: hazemhassan2@gmail.com).

Aicha Elshabini and Fred Barlow are with the Department of Electrical & Computer Engineering, University of Idaho, Moscow, ID 83844, USA (e-mail: elshabini@uidaho.edu; fbarlow@uidaho.edu).

paper [13] employs nonlinear extrapolation of Fourier data to avoid the Gibbs phenomenon and the use of windows/filtering.

In the frequency domain, a system is said to be causal if a frequency response given by the transfer function $H(w)$ satisfies the dispersion relations also known as Kramers-Krönig relations [14], [15]. The dispersion relations can be written using the Hilbert transform. They represent the fact that the real and imaginary parts of a causal function are related through Hilbert transform. The Hilbert transform may be expressed in both continuous and discrete forms and is widely used in circuit analysis, digital signal processing, remote sensing and image reconstruction [16], [6]. Applications in electronics include reconstruction [17] and correction [18] of measured data, delay extraction [19], interpolation/extrapolation of frequency responses [20], time-domain conversion [21], estimation of optimal bandwidth and data density using causality checking [22] and causality enforcement techniques using generalized dispersion relations [23], [24], [25], causality enforcement using minimum phase and all-pass decomposition and delay extraction [26], [27], [28], [29], causality verification using minimum phase and all-pass decomposition that avoids Gibbs errors [30], causality characterization through analytic continuation for L_2 integrable functions [31], causality enforcement using periodic polynomial continuations [32], [33], [34] and the subject of the current paper.

The Hilbert transform that relates the real and imaginary parts of a transfer function $H(w)$ is defined on the infinite domain which can be reduced to $[0, \infty)$ by symmetry properties of $H(w)$ for real impulse response functions. However, the frequency responses are usually available over a finite length frequency interval, so the infinite domain is either truncated or behavior of the function for large w is approximated. This is necessary since measurements can only be practically conducted over a finite frequency range and often the cost of the measurements scales in an exponential manner with respect to frequency. Likewise simulation tools have a limited bandwidth and there is a computational cost associated with each frequency data point that generally precludes very large bandwidths in these data sets. Usually $H(w)$ is assumed to be square integrable, which would require the function to decay at infinity. When a function does not decay at infinity or even grows, generalized dispersion relations with subtractions may be successfully used to reduce the dependence on high frequencies and allow a domain truncation [23], [24], [25]. A review of some previous work on generalized dispersion relations and other methods that address the problem of having finite frequency range is provided in [25].

We take another approach and instead of approximating the behavior of $H(w)$ for large w or truncating the domain, we construct a causal periodic continuation or causal Fourier continuation of $H(w)$ by requiring the transfer function to be periodic and causal in an extended domain of finite length. In [32], [33], [34], polynomial periodic continuations were used to make a transfer function periodic on an extended frequency interval. In these papers, the raw frequency responses were used on the original frequency interval. Once a periodic continuation is constructed, the spectrally accurate Fast Fourier Transform [35] implemented in FFT/IFFT routines can be used to compute discrete Hilbert transform and enforce causality. The accuracy of the method was shown to depend primarily on the degree of the polynomial, which implied the smoothness up to some order of the continuation at the end points of the given frequency domain. This in turn allowed to reduce the boundary artifacts compared to applying the discrete Hilbert transform directly to the data without any periodic continuation, which is implemented in the function `hilbert` from the popular software Matlab.

In the current work we implement the idea of periodic continuations of an interconnect transfer function by approximating this function with a causal Fourier series in an extended domain. The approach allows one to obtain extremely accurate approximations of the given function on the original interval. The causality conditions are imposed exactly and directly on Fourier coefficients, so there is no need to compute Hilbert transform numerically. This eliminates the necessity of approximating the behavior of the transfer function at infinity similarly to a polynomial continuation technique employed in [32], [33], [34], and does not require the use of Fast Fourier Transform. The advantage of the method is that it is capable of detecting very small localized causality violations with amplitude close to the machine precision, at the order of 10^{-13}, and a small uniform approximation error can be achieved on the entire original frequency interval, so it does not have boundary artifacts reported by using `hilbert` Matlab function, polynomial continuations [32], [33], [34] or generalized dispersion relations [23], [24], [25]. The performed error analysis unbiases an error due to approximation of a transfer function with a causal Fourier series from causality violations that are due to the presence of a noise or approximation errors in data. The developed estimates of upper bounds for these errors can be used in checking causality of the given data.

The paper is organized as follows. Section II provides a background on causality for linear time-translation invariant systems, dispersion relations and the motivation for the proposed method. In Section III we derive causal spectrally accurate Fourier continuations using truncated singular value decomposition (SVD). In Section IV we perform the error analysis of the method and take into account a possible noise or approximation errors in the given data. We outline an approach for verifying causality of the given data by using the developed error estimates. In Section V, the technique is applied to several analytic and simulated examples, both causal and non-causal, to show the excellent performance of the proposed method that works in a very good agreement with the developed error estimates. Finally, in Section VI we present our conclusions.

II. Causality for Linear Time-Translation Invariant Systems

Consider a linear and time-invariant physical system with the impulse response $\mathbf{h}(t, t')$ subject to a time-dependent input $\mathbf{f}(t)$, to which it responds by an output $\mathbf{x}(t)$. Linearity of the system implies that the output $\mathbf{x}(t)$ is a linear functional of the input $\mathbf{f}(t)$, while time-translation invariance means that if the input is shifted by some time interval τ, the output

is also shifted by the same interval, and, hence, the impulse response function $\mathbf{h}(t,t')$ depends only on the difference between the arguments. Thus, the response $\mathbf{x}(t)$ can be written as the convolution of the input $\mathbf{f}(t)$ and the impulse response $\mathbf{h}(t-t')$ [36]

$$\mathbf{x}(t) = \int_{-\infty}^{\infty} \mathbf{h}(t-t')\mathbf{f}(t')dt' = \mathbf{h}(t) * \mathbf{f}(t). \tag{II.1}$$

Denote by

$$\mathbf{H}(w) = \int_{-\infty}^{\infty} \mathbf{h}(\tau)\, \mathrm{e}^{-iw\tau}\, d\tau \tag{II.2}$$

the Fourier transform of $\mathbf{h}(t)$[1]. $\mathbf{H}(w)$ is also called the transfer matrix in multidimensional case or transfer function in a scalar case.

The system is causal if the output cannot precede the input, i.e. if $\mathbf{f}(t) = 0$ for $t < T$, the same must be true for $\mathbf{x}(t)$. This primitive causality condition in the time domain implies $\mathbf{h}(\tau) = 0$, $\tau < 0$, and (II.2) becomes

$$\mathbf{H}(w) = \int_{0}^{\infty} \mathbf{h}(\tau)\, \mathrm{e}^{-iw\tau}\, d\tau. \tag{II.3}$$

Note that the integral in (II.3) is extended only over a half-axis, which implies that $\mathbf{H}(w)$ has a regular analytic continuation in lower half w-plane.

Examples of physical systems that satisfy the above conditions include electric networks with $\mathbf{f}$ the input voltage, $\mathbf{x}$ the output current, $\mathbf{H}(w)$ the admittance of the network; $\mathbf{f}$ the input current, $\mathbf{x}$ the output voltage, $\mathbf{H}(w)$ the impedance; $\mathbf{f}$, $\mathbf{x}$ both power waves, $\mathbf{H}(w)$ the scattering.

For simplicity, we consider the case with a scalar impulse response $h(t)$ but the approach can also be extended to the multidimensional case for any element of the impulse response matrix $\mathbf{h}(t)$.

Very often it is assumed that $H(w)$ is square integrable [31], [19], i.e. $\int_0^{\infty} |H(w)|^2 dw < C$ for some constant C. Then one can use Parseval's theorem to show that $h(t)$ is also square integrable [36]. The converse also holds [37]. Square integrability of $H(w)$ is often related with the requirement that the total energy of the system is finite. Starting from Cauchy's theorem and using contour integration, one can show [36] that for any point w on the real axis, $H(w)$ can be written as

$$H(w) = \frac{1}{\pi i} \fint_{-\infty}^{\infty} \frac{H(w')}{w-w'} dw', \quad \text{real } w, \tag{II.4}$$

where

$$\fint_{-\infty}^{\infty} = P\int_{-\infty}^{\infty} = \lim_{\epsilon\to 0}\left(\int_{-\infty}^{w-\epsilon} + \int_{w+\epsilon}^{\infty}\right)$$

denotes Cauchy's principal value. Separating the real and imaginary parts of (II.4), we get

$$\operatorname{Re} H(w) = \frac{1}{\pi} \fint_{-\infty}^{\infty} \frac{\operatorname{Im} H(w')}{w-w'} dw', \tag{II.5}$$

$$\operatorname{Im} H(w) = -\frac{1}{\pi} \fint_{-\infty}^{\infty} \frac{\operatorname{Re} H(w')}{w-w'} dw'. \tag{II.6}$$

[1]Please note that we use an opposite sign of the exponent in the definition of the Fourier transform than in [36].

These expressions relating $\operatorname{Re} H$ and $\operatorname{Im} H$ are called the dispersion relations or Kramers-Krönig relations after Krönig [15] and Kramers [14] who derived the first known dispersion relation for a causal system of a dispersive medium. In mathematics the dispersion relations (II.5), (II.6) are also known as the Sokhotski–Plemelj formulas. These formulas show that $\operatorname{Re} H$ at one frequency is related to $\operatorname{Im} H$ for all frequencies, and vice versa. Choosing either $\operatorname{Re} H$ or $\operatorname{Im} H$ as an arbitrary square integrable function, then the other one is completely determined by causality. Recalling that the Hilbert transform is defined

$$\mathcal{H}[u(w)] = \frac{1}{\pi} \fint_{-\infty}^{\infty} \frac{u(w')}{w-w'} dw',$$

we see that $\operatorname{Re} H$ and $\operatorname{Im} H$ are Hilbert transforms of each other, i.e.

$$\operatorname{Re} H(w) = \mathcal{H}[\operatorname{Im} H(w)], \quad \operatorname{Im} H(w) = -\mathcal{H}[\operatorname{Re} H(w)].$$

For example, a function $H(w) = \frac{1}{w-i}$ is clearly square integrable and satisfies the dispersion relations (II.5), (II.6), which can be verified by contour integration. An example of a function $H(w)$ that is not square integrable but satisfies the Kramers-Krönig dispersion relations (II.5), (II.6) is provided by $H(w) = \mathrm{e}^{-iaw}$, $a > 0$. The real and imaginary parts are $\cos(aw)$ and $-\sin(aw)$, and dispersion relations (II.5), (II.6) can be verified by noting that $\mathcal{H}[\cos(aw)] = \sin(aw)$ and $\mathcal{H}[\sin(aw)] = -\cos(aw)$.

In practice, the function $H(w)$ may not satisfy the assumption of square integrability and it may only be bounded or even behave like $O(w^n)$, when $|w| \to \infty$, $n = 0, 1, 2, \ldots$. In such cases, instead of dispersion relations (II.5), (II.6), one can use generalized dispersion relations with subtractions, in which a square integrable function is constructed by subtracting a Taylor polynomial of $H(w)$ around $w = w_0$ from $H(w)$ and dividing the result by $(w-w_0)^n$. This approach makes the integrand in the generalized dispersion relations less dependent on the high-frequency behavior of $H(w)$. This may be very beneficial when the high-frequency behavior of $H(w)$ is not known with sufficient accuracy or not accessible in practice at all due to availability of only finite bandwidth data. The technique was proposed in [38], [36] and implemented successfully in [23], [24], [25] to reduce sensitivity of Kramers-Krönig dispersion relations (II.5), (II.6) to the high-frequency data.

In this paper, we take an alternative approach motivated by the example of the periodic function $H(w) = \mathrm{e}^{-iaw}$, $a > 0$, mentioned above, that is not square integrable but still satisfies Kramers-Krönig dispersion relations (II.5), (II.6). The transfer function $H(w)$ in practice is typically known only over a finite frequency interval with the limited number of discrete values and it is not periodic in general. Direct application of dispersion relations (II.5), (II.6) produces large errors in the boundary regions mainly because the high-frequency behavior of $H(w)$ is missing, unless data decay to zero at the boundary. To overcome this problem, we construct a spectrally accurate causal periodic continuation of $H(w)$ in an extended domain. A method for constructing a periodic continuation, also known as Fourier continuation or Fourier extension, which is based on

regularized singular value decomposition (SVD), was recently proposed in [39], [40], [41], [42] (see also references therein). This method allows one to calculate Fourier series approximations of non-periodic functions such that a Fourier series is periodic in an extended domain. Causality can be imposed directly on the Fourier coefficients producing a causal Fourier continuation, thus satisfying causality exactly. The Fourier coefficients are determined by solving an overdetermined and regularized least squares problem since the system suffers from numerical ill-conditioning. The resulting causal Fourier continuation is then compared with the given discrete data on the original bandwidth of interest. A decision about causality of the given data is made using the error estimates developed in Section IV.

In the next section we provide details of the derivation of causal Fourier continuations.

III. Causal Fourier Continuation

Consider a transfer function $H(w)$ available at a set of discrete frequencies from $[w_{min}, w_{max}]$, where $w_{min} \geq 0$. First, let $w_{min} = 0$, so we have the baseband case. Since equations (II.5), (II.6) are homogeneous in the frequency variable, we can rescale $[0, w_{max}]$ to $[0, 0.5]$ using the transformation $x = \frac{0.5}{w_{max}} w$ for convenience, to get a rescaled transfer function $H(x)$. The time domain impulse response function $h(t)$ is often real-valued. Hence, the real and imaginary parts of $H(w)$, as the Fourier transform of $h(t)$, and, hence, of $H(x)$, are even and odd functions, respectively. This implies that the discrete set of rescaled frequency responses $H(x)$ is available on the unit length interval $x \in [-0.5, 0.5]$ by spectrum symmetry. In some cases, the data are available only from a non-zero, low-frequency cut-off $w_{min} > 0$, which corresponds to the bandpass case. The proposed procedure is still applicable since it does not require data points to be equally spaced. The transmission line example V-C considers such situation.

The idea is to construct an accurate Fourier series approximation of $H(x)$ by allowing the Fourier series to be periodic and causal in an extended domain. The result is the Fourier continuation of H that we denote by $\mathcal{C}(H)$, and it is defined by

$$\mathcal{C}(H)(x) = \sum_{k=-M+1}^{M} \alpha_k \, \mathrm{e}^{-\frac{2\pi i}{b} kx}, \tag{III.1}$$

for even number $2M$ of terms, whereas for odd number $2M+1$ of terms, the index k varies from $-M$ to M. Throughout this paper we will consider Fourier series with even number of terms for simplicity. All presented results have analogues for Fourier series with odd number of terms. Here b is the period of approximation. For SVD-based periodic continuations b is normally chosen as twice the length of the domain on which function H is given [41]. The value $b = 2$ is not necessarily optimal and it is shown [43] to depend on a function being approximated. For causal Fourier continuations we also find that the optimal value of b depends on H. In practice, b can be varied in $1 < b \leq 4$ to get more optimal performance of the method. For very smooth functions, it is better to use a wider extension zone with $b \geq 2$, for example, $b = 2$ or $b = 4$ was enough in most of our examples. However, for functions that are wildly oscillatory or have high gradients in the boundary regions of the domain where the original data are available, a smaller extension zone with $1 < b < 2$ is recommended [39]. We used $b = 1.1$ in one of our examples. Assume that values of the function $H(x)$ are known at N discretization or collocation points $\{x_j\}$, $j = 1, \ldots, N$, $x_j \in [-0.5, 0.5]$. Note that $\mathcal{C}(H)(x)$ is a trigonometric polynomial of degree at most M.

Since $\mathrm{Re}\, H(x)$ and $\mathrm{Im}\, H(x)$ are even and odd functions of x, respectively, the Fourier coefficients

$$\alpha_k = \frac{1}{b} \int_{-b/2}^{b/2} H(x) \overline{\phi_k(x)} dx, \quad k = 1, \ldots, M,$$

are real. Here $\phi_k(x) = \mathrm{e}^{-\frac{2\pi i}{b} kx}$, $k \in \mathbb{Z}$, and $\bar{}$ denotes the complex conjugate. Functions $\{\phi_k(x)\}$ form a complete orthogonal basis in $L_2[-\frac{b}{2}, \frac{b}{2}]$, and, in particular

$$\int_{-b/2}^{b/2} \phi_k(x) \overline{\phi_{k'}(x)} dx = b \, \delta_{kk'}, \tag{III.2}$$

where $\delta_{kk'}$ is the Kronecker delta. In addition, $\overline{\phi_k}(x) = \mathrm{e}^{\frac{2\pi i}{b} kx} = \phi_{-k}(x)$.

For a function e^{-iax}, the Hilbert transform is $\mathcal{H}\{\mathrm{e}^{-iax}\} = i \, \mathrm{sgn}(a) \, \mathrm{e}^{-iax}$. Hence,

$$\mathcal{H}\{\phi_k(x)\} = i \, \mathrm{sgn}(k) \phi_k(x), \tag{III.3}$$

which implies that the functions $\{\phi_k(x)\}$ are the eigenfunctions of the Hilbert transform $\mathcal{H}$ with associated eigenvalues $\pm i$ with $x \in [-\frac{b}{2}, \frac{b}{2}]$. We will use relations (III.3) to impose a causality condition on the coefficients of $C(H)(x)$ similarly as it was done in [19] for the case of square integrable $H(w)$ where the idea of projecting on the eigenfunctions of the Hilbert transform in $L_2(\mathbb{R})$ [44] was used. In the present work, the square integrability of $H(w)$ is not required and more general transfer functions than in [19] can be considered.

For convenience of derivation, let us write $C(H)(x)$ as a Fourier series $\mathcal{C}(H)(x) = \sum_{k=-\infty}^{\infty} \alpha_k \phi_k(x)$, which will be truncated at the end to get a Fourier continuation in the form (III.1). Let $\mathcal{C}(H)(x) = \mathrm{Re}\, \mathcal{C}(H)(x) + i \, \mathrm{Im}\, \mathcal{C}(H)(x)$ and $\phi_k(x) = \mathrm{Re}\, \phi_k(x) + i \, \mathrm{Im}\, \phi_k(x)$. Since

$$\mathrm{Re}\, \phi_k = \frac{1}{2}(\phi_k + \overline{\phi}_k), \quad \mathrm{Im}\, \phi_k = \frac{1}{2i}(\phi_k - \overline{\phi}_k)$$

we obtain

$$\mathrm{Re}\, \mathcal{C}(H)(x) = \sum_{k=-\infty}^{\infty} \alpha_k \, \mathrm{Re}\, \phi_k = \frac{1}{2} \sum_{k=-\infty}^{\infty} \alpha_k (\phi_k + \overline{\phi}_k)$$

and, since $\overline{\phi_k} = \phi_{-k}$, we have

$$\mathrm{Re}\, \mathcal{C}(H)(x) = \frac{1}{2} \sum_{k=-\infty}^{\infty} \alpha_k (\phi_k + \phi_{-k}) = \frac{1}{2} \sum_{k=-\infty}^{\infty} (\alpha_k + \alpha_{-k}) \phi_k,$$

where in the last sum we changed the order of summation in the second term. Similarly, we can show that

$$\mathrm{Im}\, \mathcal{C}(H)(x) = \frac{1}{2i} \sum_{k=-\infty}^{\infty} (\alpha_k - \alpha_{-k}) \phi_k.$$

For a causal periodic continuation, we need $\operatorname{Im}\mathcal{C}(H)(x)$ to be the Hilbert transform of $-\operatorname{Re}\mathcal{C}(H)(x)$. Hence,

$$\frac{1}{2i}\sum_{k=-\infty}^{\infty}(\alpha_k-\alpha_{-k})\phi_k=-\mathcal{H}\left[\frac{1}{2}\sum_{k=-\infty}^{\infty}(\alpha_k+\alpha_{-k})\phi_k\right].$$

Employing linearity of the Hilbert transform, we get

$$\frac{1}{2i}\sum_{k=-\infty}^{\infty}(\alpha_k-\alpha_{-k})\phi_k=-\frac{1}{2}\sum_{k=-\infty}^{\infty}(\alpha_k+\alpha_{-k})\mathcal{H}[\phi_k].$$

Using (III.3), we obtain

$$\frac{1}{2i}(\alpha_k-\alpha_{-k})=-\frac{1}{2}(\alpha_k+\alpha_{-k})i\operatorname{sgn}(k)\quad\text{for any } k\in\mathbb{Z}$$

or

$$\alpha_k-\alpha_{-k}=(\alpha_k+\alpha_{-k})\operatorname{sgn}(k),\quad k\in\mathbb{Z},$$

that implies $\alpha_k=0$ for $k\le 0$ in (III.1). Hence, a causal Fourier continuation has the form

$$\mathcal{C}(H)(x)=\sum_{k=1}^{M}\alpha_k\phi_k(x)\tag{III.4}$$

where we truncated the infinite sum to obtain a trigonometric polynomial. Evaluating $H(x)$ at points x_j, $j=1,\dots,N$, $x_j\in[-0.5,0.5]$, produces a complex valued system

$$\mathcal{C}(H)(x_j)=\sum_{k=1}^{M}\alpha_k\phi_k(x_j)\tag{III.5}$$

with N equations for M unknowns α_k, $k=1,\dots,M$, $N\ge M$. If $N>M$, the system (III.5) is overdetermined and has to be solved in the least squares sense. When Fourier coefficients α_k are computed, formula (III.4) provides reconstruction of $H(x)$ on $[-0.5,0.5]$.

To ensure that numerically computed Fourier coefficients α_k are real, instead of solving complex-valued system (III.5), one can separate the real and imaginary parts of $\mathcal{C}(H)(x_j)$ to obtain real-valued system

$$\begin{aligned}\operatorname{Re}\mathcal{C}(H)(x_j)&=\sum_{k=1}^{M}\alpha_k\operatorname{Re}\phi_k(x_j),\\ \operatorname{Im}\mathcal{C}(H)(x_j)&=\sum_{k=1}^{M}\alpha_k\operatorname{Im}\phi_k(x_j).\end{aligned}\tag{III.6}$$

This produces $2N$ equations (N equations for both real and imaginary parts) and M unknowns α_k. We show below that both complex (III.5) and real (III.6) formulations give the reconstruction errors of the same order with the real formulation performing slightly better. To distinguish between the continuation $\mathcal{C}(H)$ computed using complex or real formulation, we will use notation $\mathcal{C}^C(H)$ and $\mathcal{C}^R(H)$, respectively.

Consider the real formulation (III.6) and introduce the following notation. Let $\vec{f}=\big(\operatorname{Re}H(x_1),\dots,\operatorname{Re}H(x_N),\operatorname{Im}H(x_1),\dots,\operatorname{Im}H(x_N)\big)^T$, $\vec{\alpha}=\big(\alpha_1,\dots,\alpha_M\big)^T$, where ^{T} denotes the transpose, and matrix A have entries

$$A_{jk}=\operatorname{Re}\{\mathrm{e}^{-\frac{2\pi i}{b}kx_j}\},\ j=1,\dots,N,\ k=1,\dots,M,$$

$$A_{(j+N),k}=\operatorname{Im}\{\mathrm{e}^{-\frac{2\pi i}{b}kx_j}\},\ j=1,\dots,N,\ k=1,\dots,M.$$

Similar notation can be made for the complex formulation (III.5). Then the coefficients α_k, $k=1,\dots,M$, are defined as a least squares solution of $A\vec{\alpha}=\vec{f}$ written as

$$\min_{\{\alpha_k\}}\sum_{j=1}^{2N}\left|\sum_{k=1}^{M}\alpha_kA_{jk}-f_j\right|^2,$$

that minimizes the Euclidean norm of the residual. This least squares problem is extremely ill-conditioned, as explained in [45] using the theory of frames. However, it can be regularized using a truncated SVD method when singular values below some cut-off tolerance ξ close to the machine precision are being discarded. In this work we use $\xi=10^{-13}$ as the threshold to filter the singular values. The ill-conditioning increases as M increases by developing rapid oscillations in the extended region. These oscillations are typical for SVD-based Fourier continuations. Once the system reaches a critical size that does not depend on the function being approximated, the coefficient matrix becomes rank deficient and the regularization of the SVD is required to treat singular values close to the machine precision. Because of the rank deficiency, the Fourier continuation is not longer unique. Applying the truncated SVD method produces the minimum norm solution $\{\alpha_k\}$, $k=1,\dots,M$, for which the corresponding Fourier continuation is oscillatory. The oscillations in the extended region do not significantly affect the quality of the causal Fourier continuation on the original domain and varying b can minimize their effect and decrease the overall reconstruction error, especially in the boundary domain.

Another way to make ill-conditioning of matrix problems (III.5) or (III.6) better is to use more data (collocation) points N than the Fourier coefficients M. This is called "overcollocation" [39] and makes the problem more overdetermined and helps to increase the accuracy of solutions. It is recommended to use at least twice more collocation points N than the Fourier coefficients M, i.e. $N=2M$. The convergence can be checked by keeping the number of Fourier coefficients M fixed and increasing the number of collocation points N. The overcollocation also helps with filtering out trigonometric interpolants that have very small errors at collocation points x_j but large oscillations between the collocation points [39]. In all our examples we use at least $N=2M$ as an effective way to obtain an accurate and reliable approximation of $H(x)$ over the interval $[-0.5,0.5]$.

In the multidimensional case when a transfer matrix $\mathbf{H}(w)$ is given, the above procedure can be extended to all elements of the matrix. Computing SVD is an expensive numerical procedure for large matrices. The operation count to find a least squares solution of $Ax=b$ using the SVD method with A being $N\times M$, $N\ge M$, matrix, is of the order $O(NM^2+M^3)$ [46]. The actual CPU times for computing SVD, solving a linear system in the least squares sense for real formulation as well as constructing corresponding causal Fourier continuations for various values of M used in this work, are shown in Table 2 in Section V. Computational savings can be achieved by noting that in our problem the matrix A depends only on the location of frequency points at which transfer matrix is evaluated/available, and continuation

parameters M and b but does not depend on actual values of $\mathbf{H}(w)$. Having frequency responses at N points, we can fix $N = 2M$, choose $b = 2$ as a default value and compute SVD only once prior to verifying causality. Varying $1 < b \leq 4$ or $2M < N$ for each element of $\mathbf{H}(w)$ separately, if needed, would require recomputing SVD.

IV. Error Analysis

In this section, we provide an upper bound for the error in approximation of a given function $H(x)$ by its causal Fourier continuation $\mathcal{C}(H)(x)$. The analysis of convergence of Fourier continuation technique based on the truncated SVD method was done by Lyon [43] using a split real formulation. In this work, we extend his results to causal Fourier continuations. The obtained error estimates can be employed to characterize causality of a given set of data.

A. Error estimates

Denote by $\hat{H}_M$ any function of the form

$$\hat{H}_M(x) = \sum_{k=1}^{M} \hat{\alpha}_k \phi_k(x) \tag{IV.1}$$

where $\phi_k(x) = \mathrm{e}^{-\frac{2\pi i}{b}kx}$, $k = 1, \ldots, M$, as before. Let $A = U\Sigma V^*$ be the full SVD decomposition [47] of the matrix A with entries $A_{kj} = \phi_k(x_j)$, $j = 1, \ldots, N$, $k = 1, \ldots, M$, where U is an $N \times N$ unitary matrix, Σ is an $N \times M$ diagonal matrix of singular values σ_j, $j = 1, \ldots, p$, $p = \min(N, M)$, V is an $M \times M$ unitary matrix with entries V_{kj}, and V^* denotes the complex conjugate transpose of V.

We can prove the following result.

Theorem : Consider a rescaled transfer function $H(x)$ defined by symmetry on $\Omega = [-0.5, -a] \cup [a, 0.5]$, where $a = 0.5\frac{w_{min}}{w_{max}}$, whose values are available at points $x_j \in \Omega$, $j = 1, \ldots, N$. Then the error in approximation of $H(x)$, that is known with some error ε, by its causal Fourier continuation $\mathcal{C}(H)(x)$ defined in (III.4) on a wider domain $\Omega^c = [-b/2, b/2]$, $b \geq 1$, has the upper bound

$$||H - \mathcal{C}(H + \varepsilon)||_{L_2(\Omega)} \leq (1 + \Lambda_2\sqrt{N(M-K)})$$
$$\times \left(||H - \hat{H}_M||_{L_\infty(\Omega)} + ||\varepsilon||_{L_\infty(\Omega)}\right) + \Lambda_1\sqrt{K/b}||\hat{H}_M||_{L_\infty(\Omega^c)} \tag{IV.2}$$

and holds for all functions of the form (IV.1). Here

$$\Lambda_1 = \max_{j:\ \sigma_j < \xi} ||v_j(x)||_{L_2(\Omega)}, \quad \Lambda_2 = \max_{j:\ \sigma_j > \xi} \frac{||v_j(x)||_{L_2(\Omega)}}{\sigma_j}, \tag{IV.3}$$

and functions $v_j(x) = \sum_{k=1}^{M} V_{kj}\phi_k(x)$ are each an up to M term causal Fourier series with coefficients given by the jth column of V; K denotes the number of singular values that are discarded, i.e. the number of j for which $\sigma_j < \xi$, where ξ is the cut-off tolerance.

Sketch of proof. To obtain the error bound (IV.2) we use ideas from [43] but employ a complex formulation and impose causality on Fourier coefficients. The error bound for $||H - \mathcal{C}(H)||_{L_2(\Omega)}$ is expressed in terms of the error $||H - \hat{H}_M||_{L_\infty(\Omega)}$ in approximation of a function with a causal Fourier series and $||\hat{H}_M||_{L_\infty(\Omega^c)}$ for any given causal Fourier series $\hat{H}_M$. This requires finding upper bounds for $||\mathcal{C}(H - \hat{H}_M)||_{L_2(\Omega)}$ and $||\hat{H}_M - \mathcal{C}(\hat{H}_M)||_{L_2(\Omega)}$, that estimate the error due to truncation of singular values and the effect of Fourier continuation on the error in approximation of a function with a causal Fourier series. If function H is known with some error ϵ, its effect is also included in a straightforward way. The bound for $||H - \hat{H}_M||_{L_\infty(\Omega)}$ follows from Jackson Theorems [48] that estimate the error in approximation of a periodic function with its M mode causal Fourier series $\hat{H}_M$ as a partial case. Indeed, a causal M mode Fourier series can be considered as an $2M$ mode Fourier series whose coefficients with nonpositive indices are zero. Hence, the error in approximating a b-periodic function H with k continuous derivatives with a causal M mode Fourier series, has the following upper bound:

$$||H - \hat{H}_M||_{L_\infty(\Omega)} \leq \frac{\pi}{2}\left(\frac{b}{\pi}\right)^k \left(\frac{1}{2M}\right)^k ||H^{(k)}||_{L_\infty(\Omega^c)}. \tag{IV.4}$$

Left and right singular vectors that form columns of matrices U and V are used in the derivation of the error estimates (IV.2), (IV.3) as alternatives to Fourier basis. □

As can be seen from (IV.3), Λ_1, Λ_2 and K depend only on the continuation parameters N, M, b and ξ as well as location of discrete points x_j, and not on the function H. The behavior of $\Lambda_1\sqrt{K/b}$ and $\Lambda_2\sqrt{N(M-K)}$ as functions of M can be investigated using direct numerical calculations. We do this for the case of equally spaced points x_j, $j = 1, \ldots, N$, which is typical in applications, and use $N = 2M$ with $b = 2$. Other distributions of points x_j, values of b and relations between M and N can be analyzed in a similar manner. For example, results for $b = 4$ are very similar to the case with $b = 2$. We find that while Λ_1 does not change much with M and remains small, the coefficient $\Lambda_1\sqrt{K/b}$ stays close to the cut-off value ξ for small M and increases at most to 10ξ for large M. This behavior does not seem to depend on the cut-off value ξ and the results are similar for ξ varying from 10^{-13} to 10^{-7}. The number K of discarded singular values grows with M (provided that singular values above ξ are computed accurately) since the ill-conditioning of the problem increases with M. Values of Λ_2 remain close to 1 for values M we considered. At the same time, the coefficient $\Lambda_2\sqrt{N(M-K)}$ grows approximately as $\sqrt{M}$ as M increases.

Since the error (IV.4) in approximation of a function with a causal Fourier series decays as $\mathcal{O}(M^{-k})$ and the coefficient $\Lambda_2\sqrt{N(M-K)}$ grows as $\mathcal{O}(M)$, the error bound part that is due to a causal Fourier series approximation

$$\epsilon_F \equiv (1 + \Lambda_2\sqrt{N(M-K)})||H - \hat{H}_M||_{L_\infty(\Omega)}$$

decays at least as fast as $\mathcal{O}(M^{-k+1})$. For comparison, the analogous error bound term for Fourier continuations reported in [43] is on the order of $\mathcal{O}(M^{-k+1/2})$, i.e. a causal Fourier series converges slightly slower than a standard Fourier series.

In practice, the smoothness order k of the transfer function $H(x)$ may not be known. In this case, it can be estimated by noting that the error bound ϵ_F can be written as

$$\epsilon_F \sim \tilde{C}M^{-k+1}. \tag{IV.5}$$

Taking natural logarithm of both sides, we get

$$\ln \epsilon_F \sim \ln \tilde{C} + (-k+1) \ln M, \tag{IV.6}$$

i.e. $\ln \epsilon_F$ is approximately a linear function of $\ln M$. The values of $\tilde{C}$ and k can be estimated as follows. Assume that H is known at N frequency points. Usually the number of frequency responses is fixed and it may not be possible to get data with higher resolution. Assume that the errors due to truncation of singular values (term with Λ_1) and a noise in data (term with $||\varepsilon||_{L_\infty(\Omega)}$) are small, so that the error due to a causal Fourier series approximation is dominant. Let $E_R(x)$ and $E_I(x)$ be reconstruction errors,

$$E_R(x) = \mathrm{Re}\, H(x) - \mathrm{Re}\, \mathcal{C}(H)(x), \tag{IV.7}$$

$$E_I(x) = \mathrm{Im}\, H(x) - \mathrm{Im}\, \mathcal{C}(H)(x) \tag{IV.8}$$

on the original interval $[-0.5, 0.5]$. Compute $E_R(x)$ and $E_I(x)$ with N, $N/2$, $N/4$ etc. samples, i.e. with M, $M/2$, $M/4$ etc. Fourier coefficients. Solve equation (IV.6) in the least squares sense to find approximations of $\ln \tilde{C}$ and $-k+1$, and, hence, to $\tilde{C}$ and k. Then the error term ϵ_F can be extrapolated to higher values of M using (IV.5) to see if the causal Fourier series approximation error decreases if the number M of Fourier coefficients increases, i.e. resolution increases.

The error bound term

$$\epsilon_T = \Lambda_1 \sqrt{K/b} ||\hat{H}_M||_{L_\infty(\Omega^c)}, \tag{IV.9}$$

that is due to the truncation of singular values, is typically small and close to the cut-off value ξ for small $M < 250$ and at most 10ξ for $250 \le M \le 1500$. As can be seen from (IV.9), ϵ_T depends on b and the function H being approximated. The default value $b = 2$ may not provide the smallest error. To find a more optimal value of b, a few values in $1 < b \le 4$ may be tried to determine which one gives smaller overall reconstruction errors. In case of non-causal functions, varying b does not essentially effect the size of reconstruction errors.

The error ε in data should be known in practice since the error in measurements or the accuracy of full wave simulations are typically known. The error bound term due to a noise in data

$$\epsilon_n = (1 + \Lambda_2 \sqrt{N(M-K)}) ||\varepsilon||_{L_\infty(\Omega)}$$

consists of the norm of the noise amplified by the coefficient $\Lambda_2 \sqrt{N(M-K)})$ that grows as $\mathcal{O}(M)$ as was shown above. In numerical experiments that we conducted the reconstruction errors due to a noise in data seem to level off to the order of ε and are not amplified significantly as the resolution increases. This does not contradict the error estimate (IV.2), (IV.3). The error bounds are not tight and the actual reconstruction errors may be smaller than the error bounds suggest.

B. Causality characterization

The error estimate (IV.2), (IV.3) shows that the reconstruction errors $E_R(x)$ and $E_I(x)$ defined in (IV.7), (IV.8) can be dominated by either the error due to approximation of a function with its causal Fourier series, which has the upper bound ϵ_F, or the error ϵ due to a noise or approximation errors in data, which has the upper bound ϵ_n, or if the only errors in data are round-off errors, then the reconstruction errors will approach or will be bounded by the error due to truncation of singular values, which has the upper bound ϵ_T, i.e.

$$||H - \mathcal{C}(H + \varepsilon)||_{L_2(\Omega)} \le \epsilon_F + \epsilon_n + \epsilon_T.$$

The noise level ϵ should be known in practice. In case of experimental data, ϵ could be around 10^{-3} or 10^{-4}, for example. Data obtained from finite element simulations may be accurate within 10^{-6} or 10^{-7}, for instance, which would correspond to a single precision accuracy. In some cases, the expected accuracy may be even higher. In this case if the reconstruction errors are higher than ϵ_n (in practice ϵ can be used), then the reconstruction errors may be dominated by a causal Fourier series approximation error with the upper bound ϵ_F. Determining the smoothness order of H, when only limited resolution is available, using the error model (IV.5) with N, $N/2$, $N/4$ etc. samples and extrapolating the results to higher values of M will enable one to differentiate between the causal Fourier series approximation error due to the finite number of samples and a noise or approximation errors in data, and make a decision about causality of a given set of samples with available resolution.

In the next section we employ the proposed causal Fourier continuation based method to several analytic and simulated examples that are causal/non-causal or have imposed causality violations. When a given transfer function $H(x)$ is causal, we expect that the dispersion relations (II.5), (II.6) are satisfied with the accuracy that increases with increasing resolution following the error bound ϵ_F and reaching the level close to the cut-off tolerance ξ or ϵ_T. This is so called an ideal causality test. When there is a causality violation, the reconstruction errors should level off approximately at the expected level of a noise ϵ as resolution increases. We also want to investigate whether the method is able to point to the location(s) of causality violations. We show that the results are in full agreement with the error estimates developed in Section IV.

V. Numerical Experiments: Causality Verification

A. Two-pole example

The two-pole transfer function with no delay [19] is defined by

$$H(w) = \frac{r}{iw + s} + \frac{\overline{r}}{iw + \overline{s}} \tag{V.1}$$

where $r = 1+3i$, $s = 1+2i$. Since both poles of this function located at $\pm 2 + i$ are in the upper half plane, the transfer function is causal as a linear combination of causal transforms. We sample data on the interval from $w = 0$ to $w_{max} = 6$, use the spectrum symmetry to obtain data on $[-w_{max}, 0)$ and scale the frequency interval from $[-w_{max}, w_{max}]$ to $[-0.5, 0.5]$. The real and imaginary parts of $H(x)$ are shown in Fig. 1. Superimposed are their causal Fourier continuations obtained using $M = 250$, $N = 1000$, $b = 4$ and solving the complex system (III.5) and its real counterpart (III.6). As can be seen, there is no essential difference in using complex or real formulation, though the real formulation (III.6) is slightly more ill-conditioned than the complex one. The data and the

causal Fourier continuations are practically undistinguishable on $[-0.5, 0.5]$. To demonstrate the nature of continuations, we

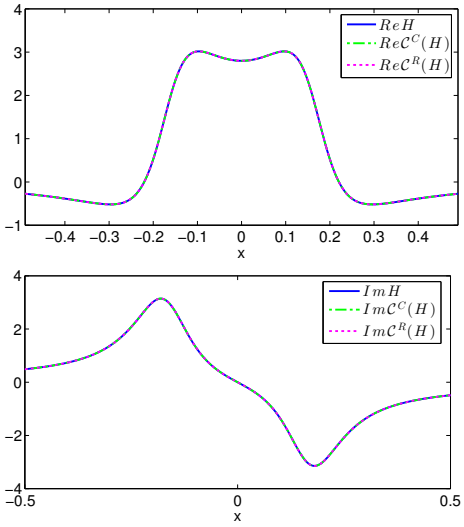

Fig. 1. $H(x)$ and its Fourier continuations $\mathcal{C}^C(H)$ and $\mathcal{C}^R(H)$ computed using complex (III.5) and real (III.6) formulations in the two-pole example V-A with $M = 250$, $N = 4M$, $b = 4$ shown on $[-0.5, 0.5]$.

plot the same curves as in Fig. 1 (only the real parts are presented, the imaginary parts have similar features) but on the extended domain $[-4, 4]$ where we show two periods. These are plotted in Fig. 2. It is obvious that the continuations oscillate in the extended region outside $[-0.5, 0.5]$. The frequency of these oscillations increases with M. At the same time, the Fourier series become more and more accurate in approximation in the original interval $[-0.5, 0.5]$. To demonstrate this, we show the reconstruction errors $E_R(x)$, defined in (IV.7), in Fig. 3 (semilogy plot is shown) in $[-0.5, 0.5]$ for various values of M with $N = 4M$ obtained using real formulation (III.6). The results for $E_I(x)$ are similar. As M increases from $M = 5$ to 250, the order of the error decreases from 10^{-1} to 10^{-14} for both real and imaginary parts. For example, with $M = 250$, $N = 1000$, $b = 4$, both errors $E_R(x)$ and $E_I(x)$ are at the order of 4×10^{-14}. The results indicate that the error is uniform on the entire interval $[-0.5, 0.5]$ and does not exhibit boundary artifacts. The above

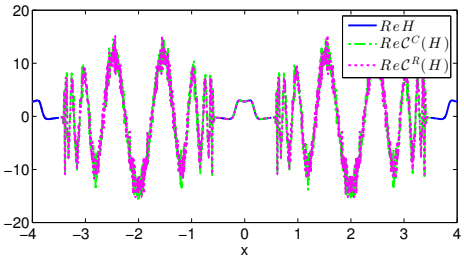

Fig. 2. The real part of Fourier continuations $\mathcal{C}^C(H)$ and $\mathcal{C}^R(H)$ in the two-pole example V-A with $M = 250$, $N = 1000$, $b = 4$ shown on a wider domain $[-4, 4]$ (two periods are shown).

results demonstrate that the proposed technique is capable of verifying that the given data are causal with high accuracy. In

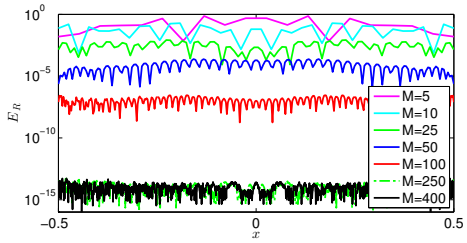

Fig. 3. Semilogy plot of the errors $|E_R(x)|$ in the two-pole example V-A on $[-0.5, 0.5]$ with $M = 5$, 10, 25, 50, 100 and 250 and 400, $N = 4M$, $b = 4$.

this case, causality is satisfied with the error less than 10^{-13}. These results are in agreement with the error estimates (IV.2), (IV.3) developed in Section IV. Indeed, since the data do not have any noise except of round-off errors and the transfer function is smooth on $[-0.5, 0, 5]$, the reconstruction errors are dominated by the fast decaying error in approximation of the smooth transfer function with its causal Fourier series (with the upper bound ϵ_F) for smaller M and then by the error due to truncation of the singular values (with the upper bound ϵ_T) for high values of M, which it is close to the cut-off value $\xi = 10^{-13}$. This is shown in Fig. 4 for E_R, where we also plot a least squares fit of the decaying part of

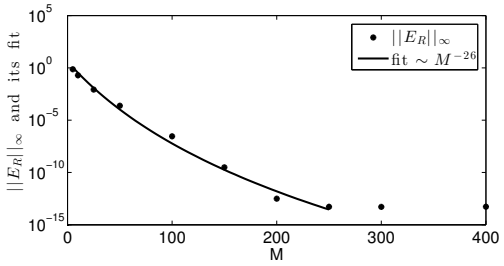

Fig. 4. Error $||E_R(x)||_\infty$ in approximation of $H(x)$ in the two-pole example V-A as a function of M with $N = 4M$ and $b = 4$, together with its least squares fit $||E_R||_\infty \sim M^{-26}$. For $E_I(x)$, we find $||E_I||_\infty \sim M^{-25.91}$.

$||E_R(x)||_\infty$ to CM^α as suggested by the error model (IV.5) and find that $||E_R||_\infty \sim M^{-26}$ indicating high smoothness rate of H and fast decay of the error due to a causal Fourier series approximation. The error E_I decays at a similar rate $||E_I||_\infty \sim M^{-25.91}$. Both errors level off at $M = 250$ by reaching the magnitude 5×10^{-14} that is close to the cut-off value ξ in filtering of singular values given by the error term ϵ_T. This result can also be interpreted that the data do not have noise of amplitude larger than 10^{-13}. We also make another observation about the behavior of the errors $E_R(x)$ and $E_I(x)$ as M increases for a causal smooth function. Even for small values of M, as M doubles, the errors decrease by several orders of magnitude until the errors level off around 5×10^{-14} (see Table 1). This is a consequence of the fast convergence of a Fourier series for a smooth function.

Next we test how sensitive this method is to causality violations. We do this by imposing a localized non-causal perturbation on causal data. This artificial causality violation

N	M	$\|\|E_R\|\|_\infty$, $\|\|E_I\|\|_\infty$	N	M	$\|\|E_R\|\|_\infty$, $\|\|E_I\|\|_\infty$
40	10	$\sim 10^{-1}$	400	100	$\sim 10^{-7}$
100	25	$\sim 4 \times 10^{-3}$	800	200	$\sim 2 \times 10^{-13}$
200	50	$\sim 10^{-4}$	1000	250	$\sim 5 \times 10^{-14}$

TABLE 1
THE ORDERS OF ERRORS $E_R(x)$ AND $E_I(x)$ IN THE TWO-POLE EXAMPLE V-A TO DEMONSTRATE HOW FAST RECONSTRUCTION ERRORS DECAY AS RESOLUTION INCREASES IN CASE OF A CAUSAL SMOOTH FUNCTION.

is modeled by a Gaussian function

$$a \exp\left(-\frac{(x-x_0)^2}{2\sigma^2}\right) \tag{V.2}$$

of small amplitude a, centered at x_0 and added to $\mathrm{Re}\, H$, while keeping $\mathrm{Im}\, H$ unchanged. This type of non-causal perturbation was used in [23] to test causality verification technique based on the generalized dispersion relations. We use the Gaussian centered at $x_0 = 0.1$ with standard deviation $\sigma = 10^{-2}/6$, so its "support" is concentrated on a very narrow interval of length 10^{-2} and outside this interval the values of the perturbation are very close to 0. The advantage of using a Gaussian perturbation is that it can be localized and allows one to verify if the proposed method is capable of detecting the location of causality violation. By varying the amplitude a, we can impose larger or smaller causality violations. The smaller a can be used, the more sensitive method is for detecting causality violations. With $a = 10^{-10}$, which gives a very small causality violation, the error between the data and their causal Fourier continuation is shown in Fig. 5. It is clear that both $E_R(x)$ and $E_I(x)$ have very pronounced spikes at $x = \pm 0.1$ due to symmetry that correspond to the exact locations of the Gaussian perturbation. These spikes are of the order 10^{-11} whereas on the rest of the interval the error is about 10 times smaller. For larger perturbations, the results are similar. For example, with $a = 10^{-8}$, the error at ± 0.1 is of the order of 10^{-9} and the rest of the interval has the error 10 times smaller, etc. We can see that the reconstruction error in this case is strongly dominated by the error (perturbation) in the data at the location of causality violation and the magnitude of the error is of the same order as the order of the perturbation. At the same time, the transfer function itself is very smooth, which ensures fast convergence of the Fourier series. Indeed, for the case with $a = 10^{-10}$, we find that the reconstruction errors decay like $||E_R(x)||_\infty \sim M^{-15.65}$ and $||E_I(x)||_\infty \sim M^{-16.91}$ until they level off at $M = 200$ with the magnitude of 5×10^{-11}. The results are in a perfect agreement with the error estimate (IV.2), (IV.3).

Another perturbation that we consider is a cosine function $a\cos(20\pi x)$ that we also add to $\mathrm{Re}\, H(x)$ but keep $\mathrm{Im}\, H(x)$ unaltered. Adding a non-causal cosine perturbation makes the transfer function non-causal on the entire interval and higher reconstruction errors are expected everywhere. We find that both errors $E_R(x)$ and $E_I(x)$ oscillate with the frequency and amplitude similar to those of the perturbation. For example, with $a = 10^{-10}$, these errors are of the order 6×10^{-11}.

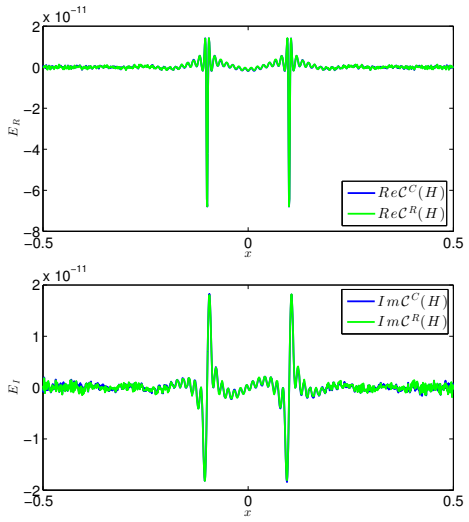

Fig. 5. Semilogy plot of $E_R(x)$ and $E_I(x)$ in the two-pole example V-A with Gaussian perturbation (V.2) with $a = 10^{-10}$ on $[-0.5, 0.5]$ with $M = 250$, $N = 1000$, $b = 4$.

Increasing/decreasing a increases/decreases the magnitude of the error. To see how the level of a noise can be detected, set, for example, $a = 10^{-5}$ and compute the reconstruction errors $E_R(x)$ and $E_I(x)$ as the resolution increases. We vary M from 10 to 400 and analyze the order of ∞ norms of these errors. The results for $E_R(x)$ are plotted in Fig. 6. As we can see, the reconstruction errors first decrease as the resolution (the number N of points) and the number M of Fourier coefficients increase until the error reaches the size 10^{-5} of the perturbation, which happens at $M = 100$, and after that the order of the error does not decrease further and levels off instead. By fitting the decreasing part of $||E_R(x)||_\infty$ to CM^α

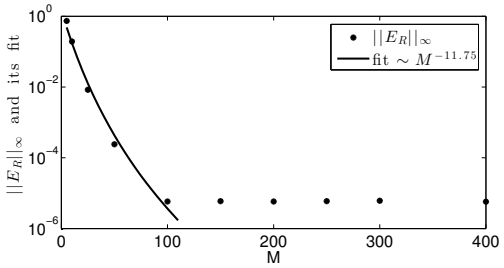

Fig. 6. Error $||E_R(x)||_\infty$ in approximation of $H(x)$ with a cosine perturbation with $a = 10^{-5}$ in the two-pole example V-A as a function of M with $N = 4M$ and $b = 4$, together with its least squares fit: $||E_R||_\infty \sim M^{-11.75}$. For $E_I(x)$, we find $||E_I||_\infty \sim M^{-11.62}$.

suggested by the error model (IV.5), we find that the errors decay like $||E_R(x)||_\infty \sim M^{-11.75}$ and $||E_I||_\infty \sim M^{-11.62}$ until they level off at $M = 100$ indicating the presence of a noise of size 10^{-5} in the data, which agrees with the error estimate (IV.2), (IV.3).

With a smaller perturbation amplitude a, the error reaches the size of the perturbation and levels off at a larger value of M. For example, with $a = 10^{-10}$, the reconstruction errors stop decreasing at $M = 200$.

B. Finite Element Model of a DRAM package

In this example we use a scattering matrix S generated by a Finite Element Modeling (FEM) of a DRAM package (courtesy of Micron). The package contains 110 input and output ports. The simulation process was performed for 100 equally spaced frequency points ranging from w_{min}=0 to $w_{max} = 5$ GHz. We expect data to be causal but, perhaps, with some error due to limited accuracy of numerical simulations. For simplicity, we apply our method to the S-parameter $S(100, 1)$ rather than the entire 110×110 S-matrix. The selected S-parameter $H(w) = S(100, 1)$ relates the output signal from port 100 to the input signal at port 1 as a function of frequency w. Our approach can be extended to the entire S-matrix by applying the method to every element of the scattering matrix S. The graph of $H(x)$ is shown in Fig. 7. In this test example, the number of samples in $[-0.5, 0.5]$

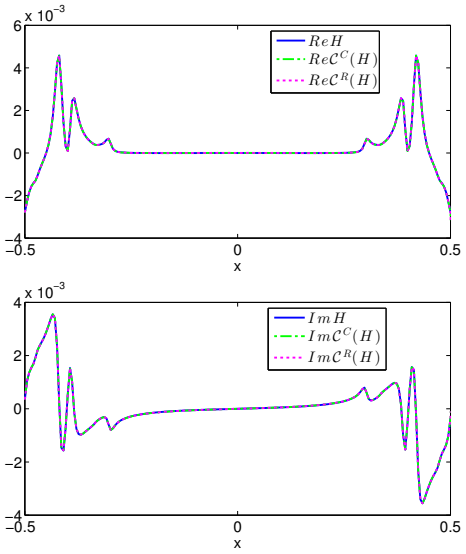

Fig. 7. $H(x)$ with its causal Fourier continuations $\mathcal{C}^C(H)$ and $\mathcal{C}^R(H)$ in the DRAM package example V-B with $M = 100$, $N = 199$, $b = 1.1$.

is fixed at $N = 2 \cdot 100 - 1 = 199$ (by symmetry), so to construct a causal Fourier continuation we use $M = 100$ Fourier coefficients and can only vary the length b of the extended region. Because the transfer function has oscillations and high slopes in the boundary region, we have to use a smaller value of b. We find $b = 1.1$ to be optimal by trying a few different values of $b \in (1, 2)$. Slightly higher values of b give similar results while using too large b does not produce small enough error, most likely because we have fixed resolution and more data points would be needed to construct a causal continuation on a larger domain with good enough resolution.

The errors $E_R(x)$ with the above parameters are shown in Fig. 8. The errors $E_I(x)$ have the same order of 10^{-5}. This implies that the dispersion relations are satisfied within error on the order of 10^{-5}. Since the data came from finite element simulations, we expect their accuracy to be on the order of 10^{-6} or 10^{-7} at least. To verify if the relatively large reconstruction errors comes from a noise in the data or a causal Fourier series approximation error, we use data with N samples, then every other and every forth samples, i.e. with N, $\frac{N-1}{2} + 1$ and $\frac{N-1}{4} + 1$ samples to find an error model (IV.5) of the form CM^{α} using the least squares method. We find that both E_R and E_I decay approximately as $\mathcal{O}(M^{-3})$. These models were extrapolated to higher values of M as shown in Fig. 9 for E_R, where we plot the ∞ norms of actual reconstruction errors and the fitted model curve. The extrapolated error curve indicates that the error may be decreased further if more frequency samples are available. In this case, we say that the transfer function $H(x)$ satisfies dispersion relations within 10^{-5}, i.e. the transfer function $H(x)$ is causal within the error at most 10^{-5}, and the causality violations, if present, are smaller than or at most on the order of 10^{-5}. To determine the actual level of a noise in the data, higher resolution of frequency responses would be needed.

For comparison, using periodic polynomial continuation method [32], [33] with 8th degree polynomial applied to the transfer function in this example, the error in approximation of $H(x)$ is about 2×10^{-3} that is by two orders of magnitude larger than with the spectral continuation, it is not uniform and the largest in the boundary domain.

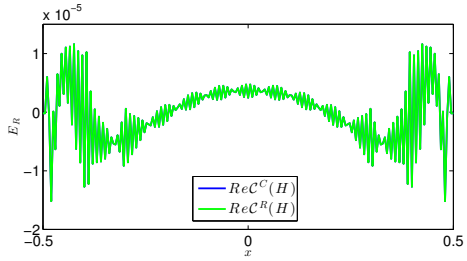

Fig. 8. Errors $E_R(x)$ in approximation of $S(100, 1)$ in the DRAM package example V-B with $N = 199$, $M = 100$ and $b = 1.1$. Errors $E_I(x)$ have the same order.

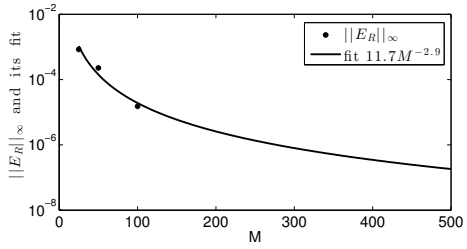

Fig. 9. Errors $||E_R(x)||_\infty$ in approximation of $S(100, 1)$ in the DRAM package example V-B with $N = 199$, 99, 49 and $M = 100$, 50, 25, respectively, and $b = 1.1$, together with their least squares fit: $||E_R||_\infty \sim 11.7M^{-2.9}$ and extrapolation for higher values of M. For $||E_I(x)||_\infty$, we find $||E_I||_\infty \sim 23.5M^{-3.1}$.

C. Transmission line example

We consider a uniform transmission line segment that has the following per-unit-length parameters: $L = 4.73$ nH/cm, $C = 3.8$ pF/cm, $R = 0.8$ Ω/cm, $G = 0$ and length $\mathcal{L} = 10$ cm. The frequency is sampled on the interval $(0, 5.0]$ GHz.

This example was used in [23] to analyze causality using generalized dispersion relations with subtractions. The scattering matrix of the structure was computed using Matlab function `rlgc2s`. Then we consider the element $H(w) = S_{11}(w)$. Due to limitation of the model used in the function `rlgc2s`, we cannot obtain the value of the transfer function at $w = 0$ (DC) but we can sample it from any small nonzero frequency. It is typical for systems to have frequency response missing at low frequencies and can occur either during measurements or simulations. However, the value of $H(w)$ at $w = 0$ is finite, because the magnitude of S_{11} must be bounded by 1. Hence, we have a bandpass case. Once we choose the number of points and the corresponding $w_{min} > 0$, we can sample frequencies from $[w_{min}, w_{max}]$. We use $w_{max} = 5.0$ GHz. Using symmetry conditions we reflect the values of the transfer function for negative frequencies as for the baseband case considered above. We know that $\mathrm{Im}\, H(w)$ equals 0 at $w = 0$ but $\mathrm{Re}\, H(w)$ is to be computed. Since we do not have a value of $\mathrm{Re}\, H(w)$ at $w = 0$, our frequencies at which the values of the transfer function are available will have a gap at $w = 0$. Nevertheless, our approach is still applicable since it does not require the data points to be equally spaced. In this example, we get better results, however, with smaller w_{min}. Alternatively, we can use a polynomial interpolation to find a value of the real part of $H(w)$ at $w = 0$. The value of the imaginary part $\mathrm{Im}\, H(0) = 0$ by symmetry. This approach is not very accurate since it does not take into account causality when the polynomial interpolation of $\mathrm{Re}\, H(w)$ is constructed, and produces a larger error compared with just skipping the value at $w = 0$ and using spectral continuation approach directly. With our technique and $M = 1500$, $N = 3000$, $b = 4$ we are able to construct a causal Fourier continuation accurate within 3×10^{-15}. The graphs of $\mathrm{Re}\, H(w)$ together with their causal Fourier continuations are presented in Fig. 10. Agreement for $\mathrm{Im}\, H(w)$ is similar. Analyzing ∞ norms of the

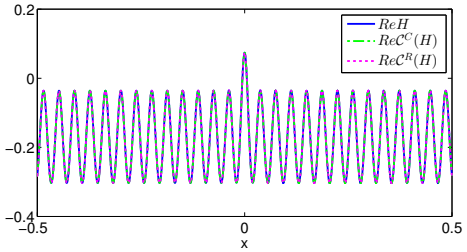

Fig. 10. Transfer function $H(x)$ and its causal Fourier continuations $\mathcal{C}^C(H)$ and $\mathcal{C}^R(H)$ in the transmission line example V-C with $M = 1500$, $N = 3000$, $b = 4$ (real parts are shown).

errors as functions of M as it was done for previous cases, we find that these errors decay as $||E_R||_\infty \sim M^{-27.05}$ and $||E_I||_\infty \sim M^{-27.28}$. They level off at $M = 250$ by reaching the magnitude of 10^{-15} indicating causality of the transfer function with high accuracy. High decay rates imply a high order of smoothness of the transfer function and that the level of a noise is close to the machine precision.

Computations presented in this paper were done using Matlab on a MacBook Pro with 2.93 GHz Intel Core 2 Duo Processor and 4 GB RAM. The CPU times (in seconds) for computing SVD, minimum norm solution of a linear system using the least squares method for real formulation and overall CPU time for constructing a causal Fourier continuation with M varying from 50 to 1500 with $N = 2M$ are shown in Table 2. Times for computing causal Fourier continuations using a complex formulation are of the same order, just slightly bigger.

M	N	CPU SVD	CPU time minnmsvd	overall CPU continuation
50	100	0.0030	3.4579×10^{-5}	0.0276
100	200	0.0094	8.4246×10^{-4}	0.0543
250	500	0.1245	0.0057	0.3574
500	1000	0.7818	0.0108	1.5224
1000	2000	6.5252	0.0455	9.3935
1500	3000	29.7123	0.0814	36.8826

TABLE 2
CPU TIMES (IN SECONDS) FOR COMPUTING SVD FOR REAL FORMULATION, FINDING A MINIMUM NORM SOLUTION AND OVERALL CPU TIME FOR CONSTRUCTING A CAUSAL FOURIER CONTINUATION FOR M VARYING FROM 50 TO 1500 WITH $N = 2M$.

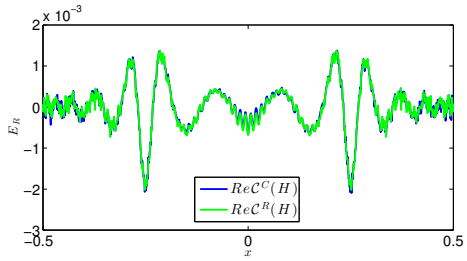

Fig. 11. Errors $E_R(x)$ in the transmission line example V-C with $M = 250$, $N = 500$, $b = 4$ and non-causal Gaussian perturbation (V.2) with $a = 10^{-2}$, $6\sigma = 0.1$, centered at $x_0 = 0.25$. The errors $E_I(x)$ have similar spikes at causality violation locations.

Now we impose a Gaussian perturbation (V.2) to the transfer function with amplitude $a = 10^{-2}$ centered at $x_0 = 0.25$ with approximate bandwidth $6\sigma = 0.1$ to model a causality violation. This perturbation is equivalent to one used in [23] after frequency rescaling. Adding the perturbation results in the error having pronounced spikes of magnitude 2×10^{-3} in both $\mathrm{Re}\, H$ and $\mathrm{Im}\, H$ at the locations of the perturbation, while the error on the rest of the interval is significantly smaller. Fig. 11 shows the error E_R in the real part. Increasing the resolution does not affect the size of the error. Analyzing ∞ norms of the errors, we find that in this case $||E_R||_\infty \sim M^{-0.26}$ and $||E_I||_\infty \sim M^{-0.13}$. Moreover, errors level off at $M = 300$ at the magnitude 2×10^{-3} indicating the presence of a noise of magnitude comparable with the magnitude of the imposed perturbation. For smaller amplitudes, higher resolution is needed to obtain accurate results since smaller amplitudes would imply higher slopes and would require more

Fourier coefficients to use. For example, with $a = 10^{-4}$, we used $M = 400$, whereas for $a = 10^{-10}$ we needed $M = 1000$.

In papers [23], [24], [25] an excellent work is done by utilizing the generalized dispersion relations with subtractions to check causality of raw frequency responses. The performed error analysis provides explicit frequency dependent error estimates to account for finite frequency resolution (discretization error in computing Hilbert transform integral) and finite bandwidth (truncation error due to using only a finite frequency interval instead of the entire frequency axis) and unbiases the causality violations from numerical discretization and domain truncation errors. It is shown that by using more subtractions, one can make the truncation error arbitrary small away from the boundary but the discretization error does not go away since it is fixed by the resolution of given frequency responses. The authors report that if causality violations are too small (with amplitude smaller than 10^{-5}) and smooth, using more subtractions may not affect the overall error since it is then dominated by the discretization error. In addition, even with placing more subtraction points in the boundary regions close to $\pm w_{max}$, the truncation error always diverges at the bandwidth edges because of missing out-of-band samples [25]. In the current work, we are able to remove boundary artifacts and detect really small localized infinitely smooth (Gaussian) causality violations as demonstrated above or even causality violations close to the boundary. In Fig. 12, we show the reconstruction error E_R for the Gaussian perturbation of amplitude $a = 10^{-2}$, located at ± 0.47, which is very close to the boundary of the domain. Because of the uniform error on the entire frequency interval, the method does not suffer from the lack of out-of-band frequencies and allows one to reliably detect localized causality violations in the boundary region as well.

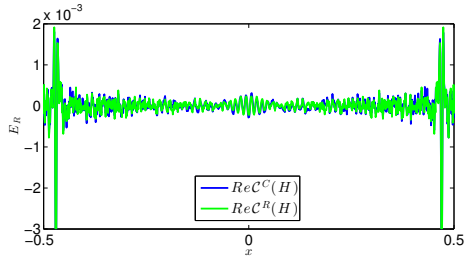

Fig. 12. Errors $E_R(x)$ in the transmission line example V-C with $M = 250$, $N = 500$, $b = 4$ and non-causal Gaussian perturbation (V.2) with $a = 10^{-2}$, $6\sigma = 0.01$, located at $x_0 = \pm 0.47$, very close to the boundary of the domain. The errors $E_I(x)$ have similar spikes at causality violation locations.

The resolution of data for the proposed method is also important since the number N of collocation points at which frequency responses are available, dictates the number M of Fourier coefficients with $N = 2M$, and, hence, the sensitivity of the method to the amplitude of causality violations.

As the support 6σ of the Gaussian narrows, the spikes in the reconstruction error at the locations of perturbations become more pronounced and easier to detected. For example, with $6\sigma = 10^{-2}$, $a = 10^{-6}$, the error E_R at the locations of the perturbation is 3×10^{-7}, whereas the error on the rest of the interval is about 10 times smaller similarly to Fig. 12. In this case, we are able to detect causality violations of amplitude up to $a = 10^{-14}$ with the same proportion between the error at causality violations and the rest of the interval.

Similarly to [25], we also find that it is more difficult to detect wide causality violations. As the "support" 6σ of the Gaussian increases, the spikes in the reconstruction errors become wider and shorter, and eventually it is not possible to determine the location of the causality violation since the error at the causality violation locations has the same order as the error on the rest of the interval. For $6\sigma \leq 0.1$, the spikes in the errors are still observable, whereas for a bigger value $6\sigma \geq 0.2$, the reconstruction errors are uniform. Increasing the resolution of the data does not decrease the reconstruction errors, once the level of a noise is reached, and reconstruction errors level off instead, which indicates the presence of causality violations and their order is approximately the order of reconstruction errors when they level off.

D. Delayed Gaussian example

Here we test the performance of the method with an example of a delayed Gaussian function that was used in [30] to check causality of interconnects through the minimum-phase and all-pass decomposition. We consider the impulse response function modeled by a Gaussian with the center of the peak t_d and standard deviation σ:

$$h(t, t_d) = \exp\left[-\frac{(t - t_d)^2}{2\sigma^2}\right].$$

If $t_d = 0$, the Gaussian function $h(t, 0)$ is even, so it cannot be causal. As t_d increases, the center of the peak moves to the right and for $t_d > 3\sigma$ the impulse response function $h(t, t_d)$ can be gradually made causal. The corresponding transfer function is

$$H(w, t_d) = \exp\left[-2(\pi w \sigma)^2 - 2i\pi w\, t_d\right]$$

which is a periodic function damped by an exponentially decaying function. We consider two regimes. One has value of $t_d < 3\sigma$, so that the transfer function $H(w, t_d)$ is non-causal. In the second regime, the delay $t_d > 3\sigma$ is big enough to make the transfer function $H(w, t_d)$ causal. We fix $b = 2$, $\sigma = 2$ and sample w from the interval $[0, 4\times 10^8]$ Hz and consider first the case with $t_d = 0.1\sigma$. The real part of $H(w, t_d)$ is shown in Fig. 13 together with its Fourier continuations. One can clearly see that Fourier continuations do not match well $\mathrm{Re}\, H$. Instead, there are visible high frequency oscillations throughout the domain as confirmed by analyzing the reconstruction errors $E_R(x)$. With $M = 250$, $N = 500$, the magnitude of the errors is about 1.1×10^{-3} (see Fig. 14). When N is increased in proportion $N = 2M$, the error slightly increases. For example, with $M = 1000$, $N = 2000$, the errors are about 1.5×10^{-3}. We also find that the errors decay like $||E_R||_\infty \sim M^{-1.6}$ and $||E_I||_\infty \sim M^{-1.78}$ and level off at $M = 100$ with the magnitude approximately 10^{-3}, indicating causality violations of that size. Varying the length b of the extended domain does not decrease the magnitude of the error. This is in agreement with the error estimate (IV.2), (IV.3) since

in this case the reconstruction error is dominated by causality violations. Results for $E_I(x)$ are similar.

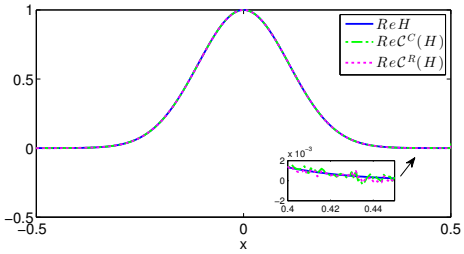

Fig. 13. Noncausal transfer function $H(w, t_d)$ in the delayed Gaussian example V-D and its Fourier continuations $\mathcal{C}^C(H)$ and $\mathcal{C}^R(H)$ with $M = 250$, $N = 500$, $b = 2$, $t_d = 0.1\sigma$ (only real parts are shown).

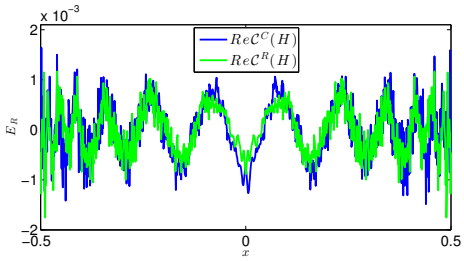

Fig. 14. Errors $E_R(x)$ between the noncausal transfer function $H(w, t_d)$ and its causal Fourier continuations $\mathcal{C}^C(H)$ and $\mathcal{C}^R(H)$ in the delayed Gaussian example V-D with $M = 250$, $N = 500$, $b = 2$, $t_d = 0.1\sigma$. Errors $E_I(x)$ have the same order.

In the second case, we set $t_d = 6\sigma$, which should give a causal transfer function. $\mathrm{Re}\, H(w, t_d)$ together with its Fourier continuations are shown in Fig. 15. Both reconstruction errors $E_R(x)$ and $E_I(x)$ are on the order of 10^{-15} as can be seen in Fig. 16. The errors decay like $||E_R||_\infty \sim M^{-79.69}$ and $||E_I||_\infty \sim M^{-79.44}$ and level off at $M = 40$ with the magnitude of 3×10^{-15}. In this case, the transfer function is causal and infinitely smooth, so the error in approximation of such a function with a causal Fourier series decays quickly to the machine precision even for moderate values of M.

We do observe a gradual change of the non-causal Gaussian function into a causal function as t_d increases. Writing $t_d = \gamma\sigma$ and vary values $\gamma = 1$, 2, 4, and 5 and find that the ∞ norms of both errors E_R and E_I are 5×10^{-6}, 10^{-7}, 3×10^{-12} and 10^{-14}, respectively, i.e. the error decays as t_d increases as expected.

VI. Conclusions

We present a numerical method for verification and enforcement, if necessary, of causality of bandlimited tabulated frequency responses, that can be employed before the data are used for macromodeling. The approach is based on the Kramers-Krönig dispersion relations and a construction of SVD-based causal Fourier continuations. This is done by calculating accurate causal Fourier series approximations of transfer functions, not periodic in general, and allowing the causal Fourier series to be periodic in an extended domain. The causality is imposed directly on Fourier coefficients using

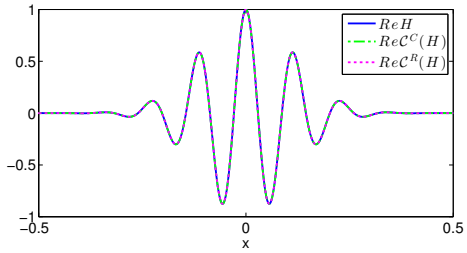

Fig. 15. Causal transfer function $H(w, t_d)$ in the delayed Gaussian example V-D and its Fourier continuation with $M = 250$, $N = 500$, $b = 2$, $t_d = 6\sigma$ (real parts are shown).

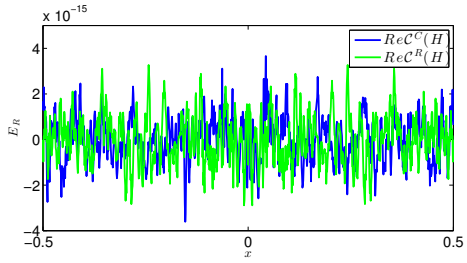

Fig. 16. Errors $E_R(x)$ between the causal transfer function $H(w, t_d)$ and its causal Fourier continuation in the delayed Gaussian example V-D with $M = 250$, $N = 500$, $b = 2$, $t_d = 6\sigma$. Errors $E_I(x)$ have the same order.

dispersion relations that require real and imaginary parts of a causal function to be a Hilbert transform pair. The approach eliminates the necessity of approximating the behavior of the transfer function at infinity, which is known to be a source of significant errors in computation of the Hilbert transform defined on an infinite domain (or semi-infinite due to spectrum symmetry) with data available only on a finite bandwidth. In addition, this procedure does not require direct numerical evaluation of the Hilbert transform. The Fourier coefficients are computed by solving an oversampled regularized least squares problem via a truncated SVD method to have the ill-conditioning of the system under control. Causal Fourier continuations even with moderate number of Fourier coefficients are typically oscillatory in the extended domain but this does not essentially affect the quality of reconstruction of the transfer function on the original frequency domain. The length of the extended domain may be tuned to find more optimal value that would allow decreasing overall reconstruction errors. The error analysis performed for the proposed method unbiases the error of approximation of a transfer function with a causal Fourier series (which decays as the resolution increases), the error due to truncation of singular values (that is close to the cut-off tolerance of singular values typically chosen close to the machine precision) from the causality violations, i.e. a noise or approximation errors in data obtained from measurements or numerical simulations (the error due to a noise has approximately the same magnitude as the noise level and may slightly grow as the resolution increases), respectively. The obtained estimates for upper bounds of these errors can be used to verify causality of the given frequency responses when only limited resolution is available. Frequency

samples with N, $N/2$, $N/4$ etc. data points can be used to estimate the order of smoothness of a transfer function, which is needed to analyze the decay of the causal Fourier series approximation error. By extrapolating the results to higher numbers of Fourier coefficients, a decision about causality of a given set of frequency samples can be made based on the available resolution. The method is applicable to both baseband and bandpass regimes and does not require data points to be equally spaced. It shows high accuracy and robustness and is capable of detecting very small localized causality violations of the amplitude close to the machine precision. The proposed technique is applied to several analytic and simulated examples with and without causality violations. The results demonstrate an excellent performance of the method in agreement with obtained error estimates.

VII. Acknowledgments

We thank the reviewers for their detailed and constructive comments. This work was funded by the Micron Foundation. The work of L.L.B. was also supported by the National Science Foundation Major Research Instrumentation Program, grant 1229766.

References

[1] M. Swaminathan and E. Engin, *Power Integrity Modeling and Design for Semiconductors and Systems*. Prentice Hall, 2007.

[2] B. Gustavsen and A. Semlyen, "Rational approximation of frequency domain responses by vector fitting," *IEEE Trans. Trans. Power Delivery*, vol. 14, no. 3, pp. 1052–1061, 1999.

[3] D. Deschrijver, B. Haegeman, and T. Dhaene, "Orthonormal vector fitting: A robust macromodeling tool for rational approximation of frequency domain responses," *IEEE Trans. Adv. Packag.*, vol. 30, no. 2, pp. 216–225, 2007.

[4] A. Charest, R. Achar, M. Nakhla, and I. Erdin, "Delay extraction-based passive macromodeling techniques for transmission line type interconnects characterized by tabulated multiport data," *Analog Integr. Circ. S.*, vol. 60, no. 1–2, pp. 13–25, 2009, 50th Midwest Symposium on Circuits and Systems, Montreal, CANADA, SEP 05-AUG 08, 2007-2008.

[5] P. Triverio, S. Grivet-Talocia, M. S. Nakhla, F. G. Canavero, and R. Achar, "Stability, causality, and passivity in electrical interconnect models," *IEEE Trans. Adv. Packag.*, vol. 30, no. 4, pp. 795–808, 2007.

[6] A. V. Oppenheim and R. W. Schafer, *Discrete-Time Signal Processing*, ser. Prentice-Hall Signal Processing Series. Prentice Hall, 1989.

[7] J.-F. Blais, M. Cimmino, A. Ross, and D. Granger, "Suppression of time aliasing in the solution of the equations of motion of an impacted beam with partial constrained layer damping," *J. Sound Vib.*, vol. 326, no. 3-5, pp. 870–882, 2009.

[8] D. Granger and A. Ross, "Effects of partial constrained viscoelastic layer damping parameters on the initial transient response of impacted cantilever beams: Experimental and numerical results," *J. Sound Vib.*, vol. 321, no. 1–2, pp. 45–64, 2009.

[9] D. Gottlieb and C.-W. Shu, "On the Gibbs phenomenon and its resolution," *SIAM Rev.*, vol. 39, no. 4, pp. 644–668, 1997.

[10] A. Gelb and J. Tanner, "Robust reprojection methods for the resolution of the Gibbs phenomenon," *Appl. Comput. Harmon. Anal.*, vol. 20, no. 1, pp. 3–25, 2006.

[11] E. Tadmor, "Filters, mollifiers and the computation of the Gibbs phenomenon," *Acta Numer.*, vol. 16, pp. 305–378, 2007.

[12] H. Mhaskar and J. Prestin, "Polynomial operators for spectral approximation of piecewise analytic functions," *Appl. Comput. Harmon. Anal.*, vol. 26, pp. 121–142, 2009.

[13] G. Beylkin and L. Monzón, "Nonlinear inversion of a band-limited Fourier transform," *Appl. Comput. Harmon. Anal.*, vol. 27, pp. 351–366, 2009.

[14] H. A. Kramers, "La diffusion de la lumiere par les atomes," *Atti Cong. Intern. Fisica (Transactions of Volta Centenary Congress) Como*, vol. 2, pp. 545–557, 1927.

[15] R. D. L. Kronig, "On the theory of dispersion of x-rays," *J. Opt. Soc. Am.*, vol. 12, no. 6, pp. 547–557, 1926.

[16] E. A. Guillemin, *Synthesis of Passive Networks: Theory and Methods Appropriate to the Realization and Approximation Problems*. New York: R. E. Krieger, 1977.

[17] S. Amari, M. Gimersky, and J. Bornemann, "Imaginary part of antennas admittance from its real part using Bodes integrals," *IEEE Trans. Antennas Propag.*, vol. 43, no. 2, pp. 220–223, 1995.

[18] F. M. Tesche, "On the use of the Hilbert transform for processing measured CW data," *IEEE Trans. Electromagn. Compat.*, vol. 34, no. 3, 1, pp. 259–266, 1992.

[19] L. Knockaert and T. Dhaene, "Causality determination and time delay extraction by means of the eigenfunctions of the Hilbert transform," in *2008 IEEE Workshop on Signal Propagation on Interconnects*, 2008, pp. 19–22, 12th IEEE Workshop on Signal Propagation on Interconnects, Avignon, France, May 12-15, 2008.

[20] S. Narayana, G. Rao, R. Adve, T. Sarker, V. Vannicola, M. Wicks, and S. Scott, "Interpolation/extrapolation of frequency domain responses using the Hilbert transform," *IEEE Trans. Microw. Theory Techn.*, vol. 44, no. 10, 1, pp. 1621–1627, 1996.

[21] S. P. Luo and Z. Z. Chen, "Iterative methods for extracting causal time-domain parameters," *IEEE Trans. Microw. Theory Techn.*, vol. 53, no. 3, 1, pp. 969–976, 2005.

[22] B. Young, "Bandwidth and density reduction of tabulated data using causality checking," in *2010 IEEE Electrical Design of Advanced Packaging and Systems Symposium (EDAPS 2010)*, 2010, pp. 1–4.

[23] P. Triverio and S. Grivet-Talocia, "A robust causality verification tool for tabulated frequency data," in *10th IEEE Workshop On Signal Propagation On Interconnects, Proceedings*, 2006, pp. 65–68, 10th IEEE Workshop on Signal Propagation on Interconnects, Berlin, Germany, May 09–12, 2006.

[24] ——, "On checking causality of bandlimited sampled frequency responses," in *PRIME 2006: 2nd Conference on Ph.D. Research In Microelectronic and Electronics, Proceedings*, Malcovati, P. and Baschirotto, A., Ed., 2006, pp. 501–504, 2nd Conference on Ph.D. Research in MicroElectronics and Electronics, Otranto, Italy, June 12-15, 2006.

[25] ——, "Robust causality characterization via generalized dispersion relations," *IEEE Trans. Adv. Packag.*, vol. 31, no. 3, pp. 579–593, 2008.

[26] R. Mandrekar and M. Swaminathan, "Causality enforcement in transient simulation of passive networks through delay extraction," in *Signal Propagation on Interconnects, Proceedings*, 2005, pp. 25–28, 9th IEEE Workshop on Signal Propagation on Interconnects, Garmisch Partenkirchen, Germany, May 10-13, 2005.

[27] ——, "Delay extraction from frequency domain data for causal macromodeling of passive networks," in *2005 IEEE International Symposium On Circuits And Systems (ISCAS), Vols 1-6, Conference Proceedings*, ser. IEEE International Symposium on Circuits and Systems, 2005, pp. 5758–5761, IEEE International Symposium on Circuits and Systems (ISCAS), Kobe, Japan, May 23-26, 2005.

[28] R. Mandrekar, K. Srinivasan, E. Engin, and M. Swaminathan, "Causal transient simulation of passive networks with fast convolution," in *10th IEEE Workshop on Signal Propagation on Interconnects, Proceedings*, 2006, pp. 61–64, 10th IEEE Workshop on Signal Propagation on Interconnects, Berlin, Germany, May 09-12, 2006.

[29] S. N. Lalgudi, K. Srinivasan, G. Casinovi, R. Mandrekar, E. Engin, M. Swaminathan, and Y. Kretchmer, "Causal transient simulation of systems characterized by frequency-domain data in a modified nodal analysis framework," in *Electrical Performance of Electronic Packaging*, 2006, pp. 123–126, 15th IEEE Topical Meeting on Electrical Performance of Electronic Packaging, Scottsdale, AZ, Oct 23-25, 2006.

[30] B. S. Xu, X. Y. Zeng, J. He, and D.-H. Han, "Checking causality of interconnects through minimum-phase and all-pass decomposition," in *2006 Conference on High Density Microsystem Design and Packaging and Component Failure Analysis (HDP '06), Proceedings*, 2006, pp. 271–273.

[31] A. Dienstfrey and L. Greengard, "Analytic continuation, singular-value expansions, and Kramers-Kronig analysis," *Inverse Problems*, vol. 17, no. 5, pp. 1307–1320, 2001.

[32] H. A. Aboutaleb, L. L. Barannyk, A. Elshabini, and F. Barlow, "Causality enforcement of DRAM package models using discrete Hilbert transforms," in *2013 IEEE Workshop on Microelectronics and Electron Devices, WMED 2013*, 2013, pp. 21–24.

[33] L. L. Barannyk, H. A. Aboutaleb, A. Elshabini, and F. Barlow, "Causality verification using polynomial periodic continuations," *J. Microelectron. Electron. Packag.*, vol. 11, pp. 181–196, 2014.

[34] ——, "Causality Enforcement of High-Speed Interconnects via Periodic

Continuations," in *The 47th International Symposium on Microelectronics, IMAPS 2014, October 14-16, 2014*, 2014.
[35] J. W. Cooley and J. W. Tukey, "An algorithm for machine calculation of complex Fourier series," *Math. Comp.*, vol. 19, no. 90, pp. 297–&, 1965.
[36] H. M. Nussenzveig, *Causality and Dispersion Relations*. Academic Press, 1972.
[37] H. Dym and H. P. McKean, *Fourier Series and Integrals*, ser. Probability and Mathematical Statistics. Academic Press, 1985.
[38] E. J. Beltrami and M. R. Wohlers, *Distributions and the Boundary Values of Analytic Functions*. Academic Press, 1966.
[39] J. P. Boyd, "A comparison of numerical algorithms for Fourier extension of the first, second, and third kinds," *J. Comput. Phys.*, vol. 178, no. 1, pp. 118–160, 2002.
[40] O. Bruno, "Fast, high-order, high-frequency integral methods for computational acoustics and electromagnetics," in *Topics In Computational Wave Propagation: Direct and Inverse Problems*, ser. Lecture Notes In Computational Science and Engineering, Ainsworth, M. and Davies, P. and Duncan, D. and Martin, P. and Rynne, B., Ed., vol. 31, 2003, pp. 43–82.
[41] O. P. Bruno, Y. Han, and M. M. Pohlman, "Accurate, high-order representation of complex three-dimensional surfaces via Fourier continuation analysis," *J. Comput. Phys.*, vol. 227, no. 2, pp. 1094–1125, 2007.
[42] M. Lyon, "Sobolev smoothing of SVD-based Fourier continuations," *Appl. Math. Let.*, vol. 25, no. 12, pp. 2227–2231, 2012.
[43] ——, "Approximation error in regularized SVD-based Fourier continuations," *Appl. Numer. Math.*, vol. 62, no. 12, pp. 1790–1803, 2012.
[44] J. A. C. Weideman, "Computing the Hilbert transform on the real line," *Math. Comp.*, vol. 64, no. 210, pp. 745–762, 1995.
[45] D. Huybrechs, "On the Fourier extension of nonperiodic functions," *SIAM J. Numer. Anal.*, vol. 47, no. 6, pp. 4326–4355, 2010.
[46] E. Anderson, Z. Bai, C. Bischof, S. Blackford, J. Demmel, J. Dongarra, J. Du Croz, A. Greenbaum, S. Hammarling, A. McKenney, and S. D., *LAPACK Users' Guide*, ser. 3rd Ed. SIAM, 1999.
[47] L. N. Trefethen and D. Bau III, *Numerical Linear Algebra*. SIAM: Society for Industrial and Applied Mathematics, 1997.
[48] E. W. Cheney, *Introduction to Approximation Theory*. AMS Chelsea Publishing, 2000.

Lyudmyla L. Barannyk received the M.S. degree in Applied Mathematics and Ph.D. degree in Mathematical Sciences from New Jersey Institute of Technology in 2000 and 2003, respectively. She has been an Assistant Professor in the Department of Mathematics, University of Idaho, since 2007. She was a Postdoctoral Assistant Professor in the Department of Mathematics, University of Michigan, from 2003 to 2007. She is also an IEEE member.

Her research interests are electrical modeling and characterization of interconnect packages, scientific computing, mathematical modeling, dimension reduction of large ODE systems, numerical methods for ill-posed problems, fluid dynamics, interfacial instability, PDEs, pseudo-spectral methods, boundary integral methods, grid-free numerical methods.

Hazem A. Aboutaleb is the Vice President and a senior researcher with the Egyptian Communication and Cryptography Research Center (ECCRC), the Egyptian Armed Forces, Cairo, Egypt. He received his B.Sc. and M.Sc. degrees in electrical and communications engineering from the Military Technical College, Cairo, Egypt, in 1994 and 2007, respectively. He was awarded a doctoral fellowship by the Egyptian government, in 2011, to join University of Idaho, Department of Electrical and Computer Engineering, from which he received his Ph.D. degree in electrical engineering in May 2014. His research interests are in the area of Microelectronics Design and Fabrication with emphasis on microelectronic chip development processes, macromodeling of microelectronics package, causality verification and enforcement of macromodels, and co-simulation methodology of power and signal integrity.

Aicha Elshabini is a Distinguished Professor, Electrical and Computer Engineering department at University of Idaho. She is a Professional Engineer and IEEE Fellow (CPMT) and IMAPS Fellow. She is the current advisor for the National Society of Black Engineers (NSBE), the Society of Women Engineers (SWE), and the International Society of Microelectronics and Electronic Packaging (IMAPS). Prior to this role, she served as the Dean of Engineering at University of Idaho and the department Head for Electrical Engineering department, and Computer Science and Computer Engineering department at University of Arkansas.

Professor Elshabini has a B.S.E.E. degree, Cairo University in Electronics & Communications, a five years academic program (British system), an M.S.E.E., University of Toledo, Ohio in Microelectronics, and a Ph.D., Electrical Engineering from the University of Colorado at Boulder in Solid State Devices and Optoelectronics, 1978.

Elshabini was awarded the 1996 John A. Wagnon Technical Achievements Award, the 2006 Daniel C. Hughes, Jr. Memorial Award, the 2007 Outstanding Educator Award, and the 2011 President Award.

Fred Barlow is a professor and the department chair in the Department of Electrical and Computer Engineering at the University of Idaho with an emphasis on electronic packaging. He is also the NGEM Center Director and Micron Endowed Professor of Microelectronics. In the past, Dr. Barlow worked for several universities, including Virginia Tech and the University of Arkansas where he held the position of associate department head.

Professor Barlow has served as the major professor for more than twenty graduate students and served as PI or Co-PI for over six million dollars of funded research engaging the microelectronics industry. Dr. Barlow has published over 100 papers and is coeditor of The Handbook of Thin FilmTechnology (McGraw Hill, 1998), as well as for the Handbook of Ceramic Interconnect Technology (CRC Press, 2007). He is also a fellow member of the International Microelectronics and Packaging Society (IMAPS) and a senior member of the Institute of Electrical and Electronic Engineers (IEEE).